Experimental study of the burning behaviors of thin-layer pool fires

OPEN ACCESS

Experimental study of the burning behaviors of thin-layer pool fires

Jinlong Zhao [1,2], Hong Huang [2*], Grunde Jomaas[3], Maohua Zhong [2], Rui Yang [2]

[1]*Faculty of Resources & Safety Engineering, China University of Mining & Technology, Beijing*

[2]*Institute of Public Safety Research, Department of Engineering Physics,*

Tsinghua University, Beijing, China

[3]*School of Engineering BRE Centre for Fire Safety Engineering, University of Edinburgh, United*

Kingdom

Abstract：

The thin-layer burning behaviors of gasoline, including the heat flux feedback to the burning surface, the penetrating thermal radiation, the temperature profile of liquid layer, and the burning rate were studied in experiments of thin-layer pool fires in square, fireproof glass trays. Experiments with four different tray sizes (side lengths of 30 cm, 40 cm, 50 cm and 60 cm) and four different initial liquid thicknesses of 6 mm, 9 mm, 12 mm and 15 mm were conducted. The results indicate that the heat flux feedback from the flame remained approximately constant, except during the ignition and extinguishment periods, and was also independent of the initial fuel thickness. The penetrating thermal radiation, on the other hand, increased with decreasing liquid layer thickness, gradually assuming rapid exponential growth. Furthermore, a boiling layer was formed during the initial burning period and its maximum depth was close to 3.0 mm. Four typical burning phases including pre-heating burning, steady burning, thin-layer burning and extinguishment were identified. The penetrating thermal radiation was the main cause of the burning rate decrease for thin-layer burning. These findings can provide a basis on which to build a real-time burning rate model for thin-layer burning.

Key words: thin-layer burning; heat flux feedback; penetrating thermal radiation; boiling layer; burning rate

1. Introduction

Statistics show that fuel leakage accidents that occur during liquid fuel transportation frequently result in thin-layer burning incidents [1-2]. The thickness of such a liquid layer is usually on the order of millimeters because the liquid is not constrained by a physical boundary, as is the case for pool fires that occur in industrial settings, where leaks are confined by barriers constructed to contain leaks [3]. The burning area increases rapidly in thin-layer burning accidents, up to a certain leakage amount, and the ensuing thermal hazards are obvious [4-5]. For example, the accidental leakage from a tanker truck carrying 3.6×10^4 liters of diesel in the Zhejiang province of China resulted in a thin-layer fire accident with a burning diameter of more than ten meters (2016) [6]. In this accident, the driver lost his life and cars in the immediate area were damaged [6]. As a result, it is meaningful to study the burning behaviors of thin-layer burning.

Because pool fires related to liquid fuels are a safety concern, extensive research has been undertaken over several decades into fundamental aspects of the steady-burning behavior of pool fires. Topics of study include flame height [7], burning rate [8] and thermal radiation [9]. In addition to these fundamental aspects, specific environmental conditions such as high pressure [10, 11], fuel thickness [12] and confined conditions [13] have also been studied. In comparison to the steady-burning of pool fires, thin-layer burning has not attracted much attention [14], even though this type of burning occurs frequently in industrial accidents [2]. Recent years, some scholars begin to show attention on thin-layer burning due to the increase number of thin-layer accidents. For example, we can find more descriptions on thin-layer burning in the third edition of *Fire*

Dynamics and the fifth edition of *SFPE Handbook of Fire Protection Engineering* [3, 14]. In these books, it is well known that the burning rate of thin-layer burning is smaller than that of pool fires. However, the reasons behind the burning rate decrease are still unclear. In thin-layer burning field, Garo et al. conducted a series of burning scale thin-layer experiments (0.15m to 2m diameter) and built an one-dimensional heat transfer model to describe the decrease in burning rate for high-boiling-point fuels (boiling points above 100 ℃) burning on water [15-16]. In his works, the radiative heat feedback was usually considered to be absorbed by the fuel surface due to opacity of crude oil [16]. Moreover, some elaborate models were also built by Inamura, Sikanen et al. and the absorption process on radiative heat feedback was considered [17-19]. However, the used absorption coefficient sometimes is usually unclear in their works and the effect caused by absorption on radiative heat feedback is still unknown. In recent studies, Vali, Farahani et al all also pointed out that the heat transfer in liquid layer and liquid motion due to uneven heating should be further studied in thin-layer burning [20-21]. More importantly, Vali stressed the radiative absorption effect on temperature distribution and on formation of vortex in the liquid layer [21]. Therefore, we need to conduct some thin-layer experiments to study the radiative heat transfer process in the liquid layer.

The purpose of this study is to improve understanding of thin-layer burning by using different scale experiments to determine the factors that are responsible for the decrease in the burning rate. Thin-layer fire experiments were conducted in square trays of different dimensions (30 cm, 40 cm, 50 cm and 60 cm), with various initial fuel thicknesses (15 mm, 12 mm, 9 mm and 6 mm). In the experiments, the heat flux feedback (HFF), the penetrating heat flux (PHF) and the temperature profile of the liquid layer (TPLL) were measured and analyzed to provide a qualitative explanation

for the variations in the thin-layer burning rate.

2. Experimental setup and models

2.1. Experimental setup

The experimental setup was designed to investigate the burning behaviors including the heat flux feedback (HFF) from the flame, the penetrating heat flux (PHF), the temperature profile in the liquid and the burning rate. A schematic of the experimental setup is shown in Fig. 1. Four configurations of custom-made square trays with side dimensions of 30 cm, 40 cm, 50 cm and 60 cm, and with an inner depth of 3.0 cm were used. The side wall and the bottom of the custom-made square trays were all made of fireproof glass (thickness = 5 mm) and stick together by fireproof adhesive. The pool bottom was transparent and some part of heat radiation can penetrate the bottom directly. The trays could be separated in two types according to the structure and function: the first was used to measure PHF and the second was used to measure HFF, as shown in Fig. 2. In order to improve the accuracy of the experiments, the glass sheet at the measurement position was replaced by a quartz glass sheet (first type) and a quartz glass cover (second type). The height of the quartz glass cover (second type) is 16 mm (in Fig. 2). The custom-made square trays were supported by four legs and each contact area between the glass and the leg was around 1 cm2. Meanwhile, asbestos was used between the bracket and the trays to reduce the heat loss due to heat conduction. Herein the trays could be considered to be exposed in the air. This method was used by Inamura et al. [15] and Hu et al. [22] to measure the HFF. The fuel used was 120# gasoline. The properties of gasoline and fireproof glass were shown in Table.1.

In the experiments, the PHF and the HFF were measured using water-cooled heat flux meters

(SBG 01) with a nearly hemispherical wide view angle and the layout is shown in Fig. 3. The maximum range of the heat flux meters is 50kW/m^2 and the accuracy is more than 95%. The temperature profile in the liquid layer was obtained using five K-type thermocouples with a diameter of 0.5 mm, which were fixed at different positions in the centerline of the liquid pool. The measurement uncertainty of these thermocouples is less than $\pm 2.2℃$ when the measurement temperature is less than 227 ℃ and the specific layout is shown in Fig. 3.

The thin layer burning platform was placed on a Sartorius load cell and an acquisition module was used to collect the data in time. The detail measurement is shown in our previous study [23]. Moreover, a digital camera (Sony HDR-XR260E) was placed in front of the experimental setup to capture the flame height and the processing method relied mainly on the flame brightness as described by Muñoz et al. [24]. A propane torch igniter was used to ignite the fuel layer.

The thin-layer burning experiments were conducted in a large-scale 30m×14m×9m (L×W×H) chamber. During the experiments, the windows and the door were closed to reduce the influence of wind, but were not sealed. The indoor temperature was 30±3 ℃ and the humidity remained around 75±10% during the experiments. Each experiment was performed twice. The specification of the experimental conditions is shown in Table 2.

2.2. Heat transfer models

To simply explain thin-layer burning behaviors, the main heat transfer mechanics for a thin-layer burning provides the basic concepts as shown in Fig. 4, which is adapted from Hamins et al. [25]. In addition, the liquid layer is divided vertically into two parts: the boiling layer (BL) and the temperature gradient layer (TGL) based on Vali's work [21].

In general, the burning rate is determined by the received net heat from the boiling layer in

which the fuel evaporates directly. According to energy conservation, the heat available at any given time for evaporation is given by Eq. (1).

$$\dot{Q}_e = \dot{Q}_{conv} + \dot{Q}_{rad} + \dot{Q}_{cond} - \dot{Q}_{heat} - \dot{Q}_{loss} - \dot{Q}_{ref} \tag{1}$$

where $\dot{Q}_e$ is the total net heat directly used to evaporate, $\dot{Q}_{conv}$ is the convection heat between the flame and the fuel layer, $\dot{Q}_{rad}$ is the HFF to the liquid layer from the flame, $\dot{Q}_{cond}$ is the heat conduction from the side wall to the liquid layer, $\dot{Q}_{heat}$ is the heat conduction from the boiling layer to the gradient temperature layer, $\dot{Q}_{loss}$ is the heat loss to the environment, $\dot{Q}_{ref}$ is the heat flux reflection off the liquid surface.

In pool fires the $\dot{Q}_{loss}$ part is considered to be negligible, since the liquid layer is thick [25, 26]. $\dot{Q}_{ref}$ is not considered in practical calculations because the ratio of $\dot{Q}_{ref}$ to $\dot{Q}_{rad}$ is small (~3%-4%) [25]. According to previous results [8, 14, 25], $\dot{Q}_{cond}$ is only considered when the burning diameter is less than 10 cm, so we ignore this term in our experiments since our burning area is larger. Therefore, the real-time burning rate of pool fires in our experiments can be rewritten as Eq. 2:

$$m''_{real-time} = (\dot{Q}_{conv} + \dot{Q}_{rad} - \dot{Q}_{heat} - \dot{Q}_{loss})\big/ Ah_v \tag{2}$$

where A is the burning area, h_v is the evaporation heat.

The heating amount is almost equal to the evaporating heat in steady burning phase for pool fires, and $\dot{Q}_{heat}$ can be expressed as:

$$\dot{Q}_{heat} = Am''_{pool} c_p \Delta T \tag{3}$$

where m''_{pool} is the steady burning rate, c_p is the heat capacity at atmospheric pressure, $\Delta T = T_{boil} - T_{amb}$, T_{boil} is the boiling point of the fuel, T_{amb} is ambient temperature. Based on Eqs. 2-3, a commonly used expression can be derived for pool fires [3, 9, 11, 14]:

$$m''_{pool} = (\dot{Q}_{conv} + \dot{Q}_{rad})/A(c_p \Delta T + h_v) \tag{4}$$

For unsteady burning, the heating part is not equal to the evaporating part and can be expressed as:

$$\dot{Q}_{heat}(t) = A \int_0^h \rho c_p (T_{t+1} - T_t) dh \tag{5}$$

where T_t, T_{t+1} is the temperature respectively at the time of t and t+1, h is the fuel thickness, ρ is the density of fuel.

Radiative feedback, the main form of heat feedback in our experiments, is given as [8, 11, 14]:

$$\dot{Q}_{rad} = A\sigma(T_f^4 - T_0^4)[1 - \exp(-kl_m)] \tag{6}$$

where σ is the Stefan–Boltzmann constant, T_f is the temperature of the flame, T_o is the surface temperature of the liquid, k is an effective absorption-emission coefficient, and l_m is the mean beam length, which is given by Drysdale [14]:

$$l_m = 3.6(\pi(D/2)^2 H)/A_s \tag{7}$$

where D is the equivalent burning diameter, H is the flame height, and A_s is the surface area of the flame.

The convection part between the vapor layer and the fuel surface can be calculated using the stagnant layer theory [27], and can be expressed as:

$$\dot{Q}_{conv} = Ah_c[\frac{\ln(1+B)}{B}](T_e - T_{boil}) \tag{8}$$

where T_e is the evaporation temperature, h_c is the convection parameter and B is the Spalding B number. The detailed calculation is given by Quintiere [27]. The $\dot{Q}_{conv}$ part gradually approaches a constant (12.5 kW/m^2) as the burning diameter increases [8, 27]. The heat feedback to the surface can therefore be written as:

$$\dot{Q}_{rad} + \dot{Q}_{conv} = 12.5A + A\sigma(T_f^4 - T_0^4)[1 - \exp(-kl_m)] \tag{9}$$

In general, the $\dot{Q}_{loss}$ part cannot be assumed to be negligible, and should be taken into account

7

in the equations for thin-layer burning [28-31]. As a result, the real-time burning rate of thin-layer

burning is given by Eq. 9.

$$m''_{real-time} = (\dot{Q}_{conv} + \dot{Q}_{rad} - \dot{Q}_{heat} - \dot{Q}_{loss})/Ah_v \qquad (10)$$

Eq. 10 will be used to discuss and analyze the entire burning process of thin-layer burning.

According to Eq. 10, the $\dot{Q}_{loss}$ term has an obvious effect on the thin-layer burning rate and

needs to be discussed in detail.

3. Results and discussion

3.1. Heat flux feedback (HFF)

The heat flux feedback from the flame plays an important role in our experimental burning scale

and the experimental results for the measured HFF to the burning surface are shown in Fig. 5. The

measured HFF increased rapidly during the initial stage and the final extinguishing stage because

the flame directly entered into the square trays at those stages. The measured HFF remained

relatively stable during most of the burning time (approximately 3/4 of the total burning time).

Similar phenomena were observed in the other experiments, indicating that the HFF was

independent of the fuel thickness in our experiments. This finding corresponds with the previous

studies of liquid burning [14, 26]. Quintiere also suggests that the HFF to the burning surface can

be considered to be a constant, as long as the flame is tall (H > 2D) and does not change color [26].

The flame height in the experiments is obtained by analyzing RGB values of the flame pictures,

the detailed processing method is provided by Muñoz et al. [24]. Although the flame height

appeared to decrease to a certain extent (<30%) with the fuel thickness decreasing in the

experiments, the flame height was still more than twice the equivalent burning diameter except for

during the initial and final stages. In addition, there is not a strong correlation between HFF ($\dot{Q}_{rad}$)

and flame height (*H*) according to Eqs. 6 & 7. As a result, it is clearly shown that the variation of HFF is not a main reason to result from the burning rate decrease in thin-layer burning and the HFF to the burning surface can be considered to be a constant.

The measured HFF values at the center position for the different sized trays are shown in Fig. 6. We found that the measured HFF to the burning surface (in the same tray) can also be considered to be a constant for the majority of the burning time, independent of the fuel thickness for thin-layer burning. Furthermore, the measured HFF increased from approximately 11 kW/m^2 to approximately 29 kW/m^2 with the side length increasing from 30 cm to 60 cm respectively. These results correspond with the experimental findings of Ditch et al. [8].

3.2. Penetrating heat flux (PHF)

The transfer process of the radiative heat feedback from flame is shown in Fig. 7. The radiative heat feedback is mainly two parts: the absorption part by fuel ($q_{ab} + q_{refg}$) and the penetrating part measured by the heat flux meters (q_{peg}). In the transfer process, the refection part by fuel surface is usually ignored (less than 4%) [25]. Moreover, the reflection by the glass (q_{refg}) is considered to be absorbed by the fuel layer and the radiative absorption by glass is ignored due to a good transmittance. In Fig. 8, it is obvious that the penetrating heat flux is a form to result from the heat loss for liquid layer. The experimental data in Fig. 8 show that the PHF increases as the fuel thickness decreases exponentially. This illustrates that the thinner the fuel layer, the more the heat loss due to radiative transmission through the fuel layer. For example, the PHF reaches approximately 11 kW/m^2 when the fuel thickness is around 2 mm (side length is 50 cm) and the corresponding measured HFF is around 22 kW/m^2, which means more than half of the HFF is directly lost at this time. In fact, the fuel thickness is usually less than 2 mm in thin-layer burning

accidents [27-28]. We can therefore conclude that the PHF plays an important role in the heat loss for thin-layer burning accidents. Furthermore, the variation in the PHF indicates that the majority of the HFF is absorbed by the upper layer, which agrees with the experimental results of Suo-Anttila et al. [29].

In Fig. 8, we can observe that the curves of the PHF almost overlap when the fuel thickness is less than 6 mm for a fixed scale burning. For example, the PHF values are all approximately 9 kW/m^2 when the fuel thickness is around 4 mm for the experiments with a side length of 60 cm. This suggests that the penetrating property remains stable and is unrelated to the initial fuel thickness. At present, it is difficult to build an accurate model to calculate the PHF, due to the complexity of infrared waves emitted from flame and their corresponding transmission properties [15, 29]. As a result, the stable property of heat transmission can provide a fitting way to calculate the mass of the penetrating radiation. It therefore can simplify the calculation of heat loss due to penetrating radiation in practical applications.

3.3. Temperature variation

In the study five thermocouples were used to obtain the temperature distribution of the fuel layer vertically as shown in Fig. 3. The experiments with an initial liquid thickness of 15 mm were used to analyze the temperature variation in the liquid layer as shown in Fig. 9. The fuel thickness was not controlled and the position of thermocouples was fixed in the experiments. So the temperature measured by the thermocouples actually reflected the liquid temperature during the primary burning period, and then gradually became the vapor temperature as the liquid level decreased. Finally, the temperature increased rapidly because the flame entered the inner tray and touched the thermocouples directly. This entire process is clearly shown in Fig. 9. In addition, we

also found that the temperature in the liquid layer could exceed the liquid's surface temperature (boiling point). The temperature reached boiling point at first, continued to increase and then returned back to the boiling point. This trend was observed by all the thermocouples except T1 due to the boundary limitation. By analyzing the PHF, we have shown that the inner liquid part below the liquid surface absorbed a large proportion of HFF followed by a temperature increase. However, the inner part is not able to evaporate directly due to the limitation of the upper layer, resulting in superheating (over the boiling point).

In general, superheating can lead to buoyancy-driven convection in the inner liquid layer, as shown in a previous study [30]. To explain the phenomenon of temperature decrease after superheating, the Rayleigh and Nusselt numbers are introduced [30, 31]:

$$Ra = \frac{g\beta}{v\alpha}\Delta T_h h^3 \tag{11}$$

$$Nu_L = CRa^n \tag{12}$$

where g is the gravitational acceleration, β, v and α are volume expansion, kinematic viscosity and thermal diffusivity of the liquid respectively, h is the thickness of the fuel, ΔT_h is the vertical temperature difference, C and n are constants (C=0.54, n=0.25, (10^4<Ra<10^7) and C=0.15, n=1/3, (10^7<Ra<10^{11})) given by Frank [30]. The main component of 120# gasoline is heptane. The related parameters including viscosity and density are given by De la Porte and Kossack [32]. The temperature variation at the T5 position in Test 1 is used to calculate both the Rayleigh number and the Nusselt number. Figure 10 shows the variation of the Rayleigh and Nusselt numbers over burning time (65 s -105 s).

In Fig. 10, the Rayleigh number and the Nusselt number can be seen to increase rapidly when the inner liquid temperature exceeded the boiling point, indicating the forming process of the

Rayleigh convection in the liquid layer. With the increase of the Rayleigh convection, the temperature of the upper layer would gradually become uniform, which has been verified by the subsequent temperature decrease shown in Fig. 9. In addition, vortices, as a basic form of the Rayleigh convection were observed by the Particle Image Velocimetry (PIV) technique in Vali et al.'s experiments and Farahani et al.'s experiments [20, 32], which agreed with our observation of transient superheat. As the burning continued, the Rayleigh number and the Nusselt number began to decrease after 90s, as can be seen in Fig. 10, due to the decrease in the liquid thickness.

The thickness of the boiling layer is associated with the amount of evaporating fuel. By using the positions of the liquid surface and the thermocouples, we can determine the thickness of the boiling layer. For example, the thickness of boiling layer equals to that the real-time liquid thickness minus the height of the T5 thermocouple when the measured temperature by the T5 thermocouple first increases to the boiling point temperature for the experiments with initial thickness of 15 mm. Fig. 11 shows the change in the thickness of the boiling layer over the burning time in Test 1. Y is the liquid thickness and X is the distance to the center axis of the pool along the tray side. The temperature contours are plotted with linear interpolation in the X and Y directions. In Fig. 11, the liquid layer is divided into two layers: the boiling layer and the temperature gradient layer, which corresponds to the previous observation by Vali et al. [21]. After ignition, the thickness of the boiling layer increased with burning time due to the HFF from the flame. It then approached a constant thickness (~3mm) due to the absorbing ability of the fuel. The detailed relationship between the boiling layer thickness and the burning time is shown in Fig. 12. As shown in Fig. 12, the thickness of the boiling layer increased after ignition because of the absorption of the HFF. However, the maximum thickness of the boiling layer is around 3.4 mm,

independent of the burning diameter when the initial fuel thickness is 15 mm. This trend illustrates that the absorbing process occurs only in a certain range of the liquid layer, which accords with the observation of PHF, also corroborated by the previous study [29]. Suo-Anttila et al. observed that the fuel thickness of the boiling layer was around 3 mm for a large scale burning with a diameter of 2 m [29]. Compared with their work, the heat conduction from the side walls in our experiments probably accounts for the small differences noted.

On the contrary, the thickness of the boiling layer was limited by the initial fuel thickness and the boundary conditions. From the experimental data, it can be seen that the boiling layer thickness was less than 1.8 mm when the initial fuel thickness was 6 mm. The decrease in the boiling layer indicated that the amount of evaporating fuel would decrease in thin-layer burning. As a result, forming a stable boiling layer boiling layer can be used to judge whether a burning belongs to the thin-layer burning category.

In addition, the temperature of the bottom glass surface was measured by patch thermocouples in the experiments. The temperature variation of the center bottom glass with the burning time is shown in Fig. 13. At initial burning stage after ignition, the bottom fuel layer's temperature changed small and nearly kept stable because most of heat feedback was absorbed by upper fuel layer, as shown in Figs. 9 and 13. However, the temperature of bottom liquid layer had almost achieved the boiling point at later burning stage ($t/t_{total} > 0.8$) in Fig. 9. At that time, the heat conduction quantity from liquid layer to glass increased quickly, resulting from the bottom glass temperature rapidly increase, shown in Fig. 13. In the experiments, the temperature gradient was less than 0.93 K/s. The maximum heat absorbed quantity could achieve around 4.89 kW/m^2 if the vertical temperature distribution of inner glass was simplified as a linear relation. At that moment,

the heat flux penetration was more than 15 kW/m^2 and would continue to increase. Therefore, the heat flux penetration is mainly responsible for the burning rate decrease of thin-layer burning in the experiments.

3.4. Burning rate

The burning rate is related to the thickness of the fuel layer according to Eq. 9. The experiments with a side length of 30 cm are used as examples to show the detailed variation of the burning rate with the burning time. These results are shown in Fig. 14.

According to the curves of burning rate in Fig. 14, the entire burning process can be divided into four phases: (1) pre-heating burning, (2) steady burning, (3) thin-layer burning and (4) extinguishment. In the pre-heating burning phase, the burning rate increases obviously with burning time. This phase, the HFF to the fuel layer heats mainly the liquid fuel, which means $\dot{Q}_{heat}$ would account for a large proportion of the heat feedback to fuel layer. Hence, we find that the thickness of the boiling layer gradually increases in this burning phase (combined with Fig. 11). In the steady burning phase, the burning rate remains relatively stable, because the HFF, the heat loss and the thickness of the boiling layer all remain relatively stable. In the thin-layer burning phase, the burning rate decreased with the decrease in fuel thickness, which is related to initial fuel thickness. During this phase, we find that $\dot{Q}_{loss}$, particularly the PHF, gradually plays an important role in the decrease in burning rate (see Fig. 8). According to Eqs.1-10, the net heat absorbed by the boiling layer decreased sharply during this period. We should also mention that the burning rate can be affected by many factors in Eq. 1, including side wall material, fuel temperature, fuel types, etc. For this reason there are some differences between our observations and those in Chen's experiments (boiling burning phase) because of the burning scale and the

material of the trays [33].

Based on Fig. 12 and Fig. 14, it can be found that the thickness of boiling layer is closely related to the burning rate. For some experimental groups with the initial thickness of 12 mm and 15 mm, the maximum boiling layer thickness could achieve around 3 mm and sustain this value for some time in burning, which kept consistent with the burning rate's variation. In addition, the thickness of boiling layer was less than 3 mm during entire process for the experiments with the initial thickness of 6 mm and 9 mm. The maximum burning rate also decreased obviously compared with that of deeper liquid layer groups. Therefore, forming a stable boiling layer can be considered as a symbol of the steady burning phase.

4. Conclusion

A series of experiments were conducted on thin-layer burning in four different-sized square trays with four different initial fuel thicknesses. The heat flux feedback to the fuel surface, the penetrating thermal radiation and the temperature profile of the liquid layer were all analyzed. The major conclusions are:

(1) According to the variations in the burning rate, the entire burning period can be divided into four phases: pre-heating burning, steady burning, thin-layer burning and extinguishment. It should be noted that not every burning phase will appear in every experiment, which do appear is dictated by the initial fuel layer thickness.

(2) The burning rate is dependent on the initial liquid thickness for thin-layer burning, which is associated with the thickness of boiling layer. The maximum thickness of boiling layer is approximately 3 mm due to absorption of radiative feedback from flame. It is considered as a criterion to distinguish the pool and the thin-layer to form the maximum and stable boiling layer

thickness.

(3) The heat flux feedback to the fuel surface remains stable for the majority of the burning time and is independent of the initial fuel thickness. However, the penetrating heat flux obviously increases as the fuel layer decreases, which is mainly responsible for the decrease in the burning rate for thin-layer burning.

(4) In the liquid burning process, the inner liquid temperature can exceed the surface temperature for some time due to absorption of heat flux, and then decrease to the boiling point due to the increase in Rayleigh convection. The heat convection in the upper layer leads to the formation of boiling layer.

These results show the importance of thermal radiative penetration on the decrease in burning rate for thin-layer burning. However, further work should be done to analyze the absorption coefficient and the boiling layer. PIV will be used to study the fluid motion for thin-layer burning in the near future.

References：

[1] Z. Nivolianitou, M. Konstandinidou, C. Michalis, Statistical analysis of major accidents in petrochemical industry notified to the major accident reporting system (MARS), J. Hazard. Mater. 137 (2006) 1-7.

[2] H. Zhang, X. Zheng, Characteristics of hazardous chemical accidents in China: A statistical investigation, J. Loss Prev. Process Ind. 25 (2012) 686-693.

[3] D. Gottuk, D. White, Liquid Fuel Fires, In: Morgan JH, editors, The SFPE Handbook of Fire Protection Engineering (5th ed.), Springer, 2015.

[4] J. Fay, Model of spills and fires from LNG and oil tankers, J. Hazard. Mater, 96 (2003) 171-188.

[5] V. Cozzani, G. Gubinelli, G. Antonioni, G. Spadoni, S. Zanelli, The assessment of risk caused by domino effect in quantitative area risk analysis, J. Hazard. Mater. 127 (2005) 14-30.

[6] X. Chen, A spill fire accident occurred that was caused by a car accident in Zhejiang Province, Available from: http://www.zj.xinhuanet.com/zjnews/20161018/3492157_c.html, 2016, 10, 18.

[7] S. Li, Modeling of pressure effects on flame structure and soot formation of n-heptane/air co-flow laminar flames by skeletal reaction mechanism, Appl. Therm. Eng. 106(2016) 1458-1465.

[8] B. Ditch, J. de Ris, T. Blanchat, M. Chaos, R. Bill Jr, S. Dorofeev, Pool fires-An empirical correlation, Combust Flame 160 (2013) 2964-2974.

[9] L. Hu, S. Liu, L. Wu, Flame radiation feedback to fuel surface in medium ethanol and heptane pool fires with cross air flow, Combust. Flame 160(2013):295-306.

[10] J. Ji, F. Guo, Z. Gao, J. Zhu, J. Sun, Numerical investigation on the effect of ambient pressure on smoke movement and temperature distribution in tunnel fires, Appl. Therm. Eng. 118 (2017) 663-669.

[11] A. Karataş, G. Intasopa, Ö. Gülder, Sooting behaviour of n-heptane laminar diffusion flames at high pressures, Combust. Flame 160 (9) (2013) 1650-1656.

[12] A. Vali, D. Nobes, L. Kostiuk, Fluid motion and energy transfer within burning liquid fuel

pools of various thicknesses, Combust. Flame 162 (4) (2014) 1477-1488.

[13] P. Zhang, X. Tang, X. Tian, et al, Experimental study on the interaction between fire and water mist in long and narrow spaces, Appl. Therm. Eng. 94(2016) 706-714.

[14] D. Drysdale, An Introduction to Fire Dynamics (3nd ed.), John Wiley & Sons, Ltd, New York, 2011.

[15] J. Garo, J. Vantelon, H. Koseki, Thin-layer boilover: prediction of its onset and intensity, Combust. Sci. Technol. 178 (2006) 1217-1235.

[16] J. Garo, P. Gillard, J. Vantelon, A. Fernandez, Combustion of Liquid Fuels Spilled on Water. Prediction of Time to Start of Boilover, Combust. Sci. Technol. 147 (1999) 39-59.

[17] T. Inamura, K. Saito, K. Tagavi, A study of boilover in liquid pool fires supported on water. Part II: effects of in-depth radiation absorption, Combust. Sci. Technol. 86 (1992) 105-119.

[18] T. Sikanen, S. Hostikka, Modeling and simulation of liquid pool fires with in-depth radiation absorption and heat transfer, FIRE SAFETY J. 80 (2016) 95-109.

[19] B. Kozanoglu, F. Ferrero, M. Muñoz, et al., Thermal analysis of thin layer boilover, Heat Mass Transfer 44(12)(2008) 1549-1555.

[20] H. Farahani, G. Jomaas, A. Rangwala, Effects of convective motion in n-octane pool fires in an ice cavity, Combust. Flame 162 (2015) 4643-4648.

[21] A. Vali, Investigation of the transport phenomena within the liquid phase of a methanol pool fire, Ph. D. Thesis, University of Alberta, Canada, 2014.

[22] L. Hu, S. Liu, L. Wu, Flame radiation feedback to fuel surface in medium ethanol and heptane pool fires with cross air flow, Combust. Flame 160 (2013) 295-306.

[23] J. Zhao, H. Huang, H. Wang, et al. Experimental study on burning behaviors and thermal

radiative penetration of thin-layer burning. J. Therm. Anal. Calorim. 4 (2017)1-10.

[24] M. Munoz, J. Arnaldos, J. Casal, E. Planas, Analysis of the geometric and radiative characteristics of hydrocarbon pool fires, Combust. Flame 139 (2004) 263-277.

[25] A. Hamins, T. Kashiwagi, R. Burch, Characteristics of pool fire burning. In: Fire resistance of industrial fluids, ASTM International, 1995.

[26] J. Quintiere, Fundamentals of Fire Phenomena, Wiley, West Sussex, 2006.

[27] J. Zhao, H. Huang, Y. Li, B. Su, N. Zhang, Experimental and modeling study of the behavior of a large-scale spill fire on a water layer, J. Loss Prev. Process. Ind. 43 (2016) 514-520.

[28] J. Zhao, Q. Liu, H. Huang, R. Yang, H. Zhang, Experiments investigating fuel spread behaviors for continuous spill fires on fireproof glass, J. Fire Sci. 35 (2017) 80-95.

[29] J. Suo-Anttila, T. Blanchat, A. Ricks, A. Brown, Characterization of thermal radiation spectra in 2m pool fires, Proc. Combust. Inst. 32 (2009) 2567-2574.

[30] P. Frank, D. DeWitt, Fundamentals of heat and mass transfer (5th ed.), NewYork,Wiley, 2001.

[31] H. Farahani, G. Jomaas, A. Rangwala, Effects of convective motion in n-octane pool fires in an ice cavity, Combust. Flame 162 (2015) 4643-4648.

[32] J. De la Porte, C. Kossack, A liquid phase viscosity-temperature model for long-chain n-alkanes up to $C_{64}H_{130}$, based on the Free Volume Theory, Fuel 136 (2014) 156-164.

[33] B. Chen, S. Lu, C. Li, Q. Kang, V. Lecoustre, Initial fuel temperature effects on burning rate of pool fire, J. Hazard. Mater. 188 (2011) 369-374.

Table1: Properties of 120# gasoline and the fireproof glass

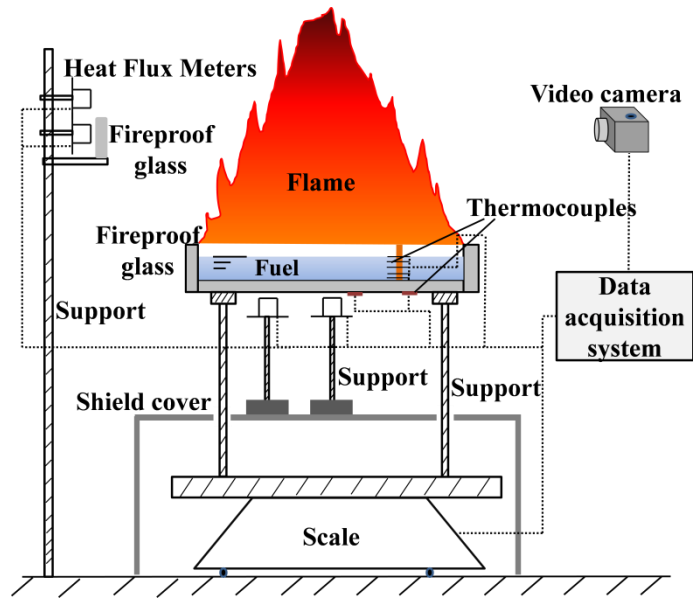**Table2**: Specification of the experimental conditions

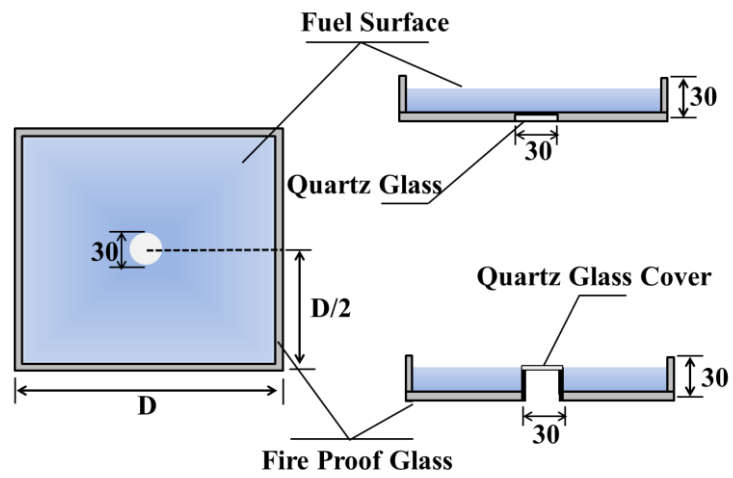**Figure 1:** Schematic of the experimental setup.

Figure 2: Detailed structure of the two types of pans. The numbered dimensions are in mm.
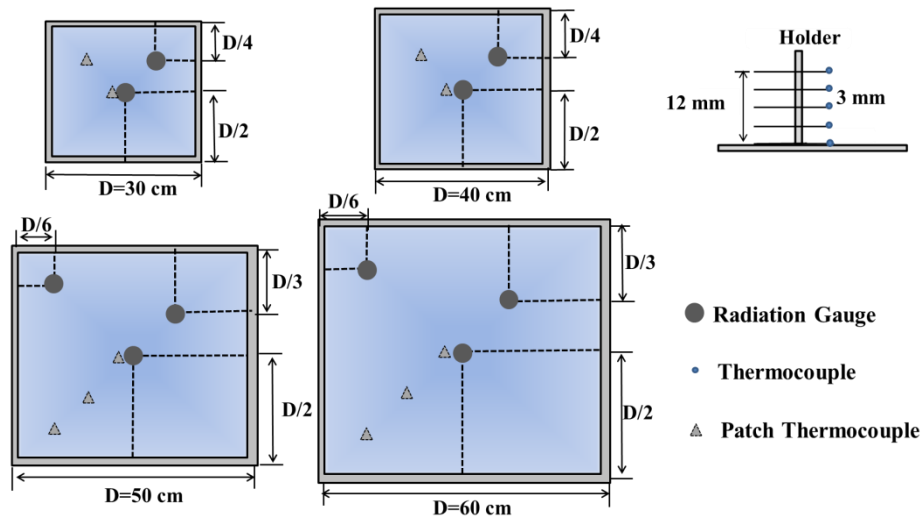
Figure 3: The specific positions of the heat flux meters, patch thermocouples and K-type thermocouples

Figure 4: Schematic of the main heat transfer mechanics and the liquid layer's temperature structure for a thin-layer burning. Adapted from Hamins et al. [28] and Vali et al. [25].

Figure 5: Experimental data of the measured HFF for different initial fuel thicknesses. Th is the initial thickness and the side length of the tray is 30 cm. **1/2 and 1/4 position means the layout position of heat flux meters corresponding to the layout in Fig. 3.**

Figure 6: Experimental results for the measured HFF for four different burning sizes. Side length refers to side length of trays.

Figure 7: The transfer process of the radiative heat feedback from flame.

Figure 8: The PHF variation vs. the fuel thickness at the center position. Th is the initial fuel thickness and Side is the side length of the tray.

Figure 9: The fuel and gas temperature and the fuel thickness variation vs. the burning time. Side is the side length of trays.

Figure 10: The change in Rayleigh number and Nusselt number over burning time.

Figure 11: The thickness of the boiling layer in Test 1. The initial fuel thickness is 15 mm and the side length of the tray is 30 cm.

Figure 12: The thickness variation of the boiling layer over the burning time. **Side is the side length of trays.**

Figure 13: The temperature variation of the center bottom glass with the burning time. Side is the side length of trays.

Figure 14: Burning rate and fuel thickness vs. burning time. The side length of the tray is 30 cm.

Table 1. Properties of 120# gasoline and the fireproof glass used in the experiments

Material	Specific heat capacity (kJ/(kg · K))	Density(15 °C) (kg/m^3)	Boiling point (°C)
120# gasoline	2.12	730	86
Fireproof glass	0.84	2500	/

Table 2. Specification of the experimental conditions

No.	Side (cm)	Initial Fuel Layer Thickness (mm)	Pan type*	No.	Side (cm)	Initial Fuel Layer Thickness (mm)	Pan type*
1	30	15	1	17	50	15	1
2			2	18			2
3	30	12	1	19	50	12	1
4			2	20			2
5	30	9	1	21	50	9	1
6			2	22			2
7	30	6	1	23	50	6	1
8			2	24			2
9	40	15	1	25	60	15	1
10			2	26			2
11	40	12	1	27	60	12	1
12			2	28			2
13	40	9	1	29	60	9	1
14			2	30			2
15	40	6	1	31	60	6	1
16			2	32			2

*The burning pans were of two types: type 1 in the table was used to measure the PHF with a quartz glass sheet and type 2 was used to measure HFF with a quartz glass cover (see Fig.2).

Fig. 1 Schematic of the experimental setup.

Fig. 2 Detailed structure of the two types of pans. The numbered dimensions are in mm.

Fig. 3 The specific positions of the heat flux meters, patch thermocouples and K-type thermocouples
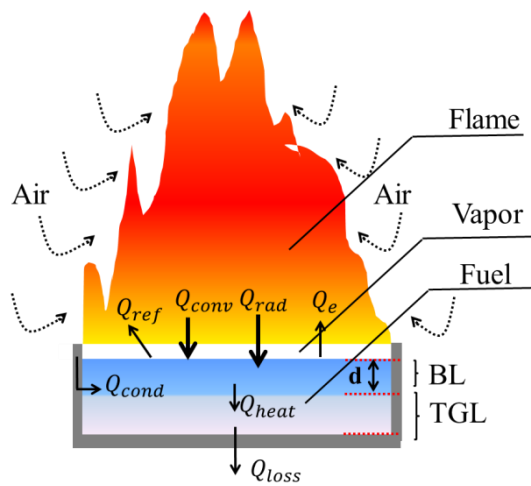
Fig. 4 Schematic of the main heat transfer mechanics and the liquid layer's temperature structure for a thin-layer burning. Adapted from Hamins et al. [24] and Vali et al. [20].
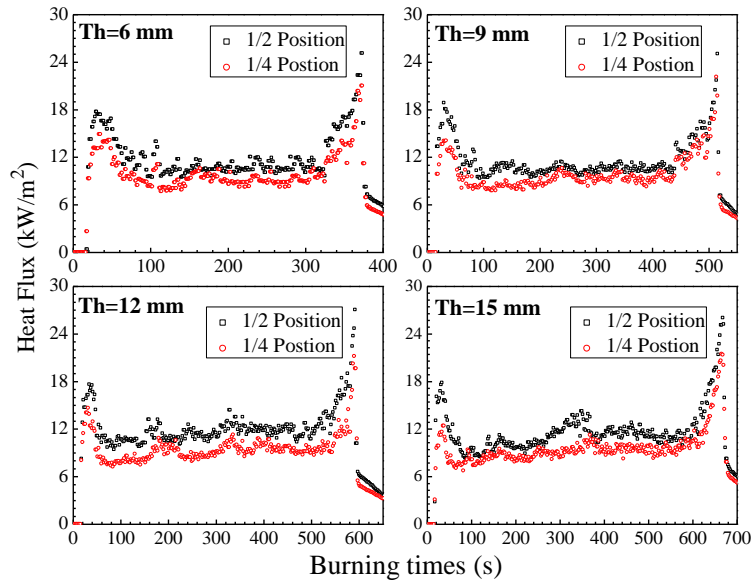
Fig. 5 Experimental data of the measured HFF for different initial fuel thicknesses. Th is the initial thickness and the side length of the tray is 30 cm. 1/2 and 1/4 position means the layout position of heat flux meters under the glass corresponding to the layout in Fig. 3
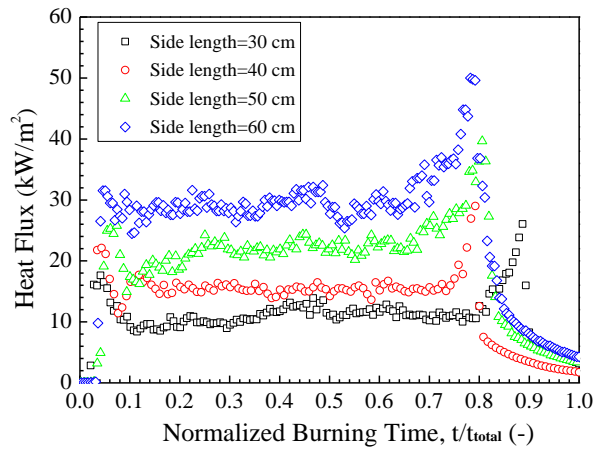
Fig. 6 Experimental results for the measured HFF for four different burning sizes. Side length refers to side length of trays.
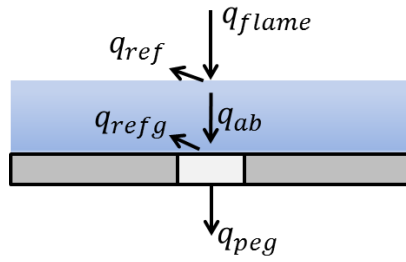
Fig. 7 The transfer process of the radiative heat feedback from flame
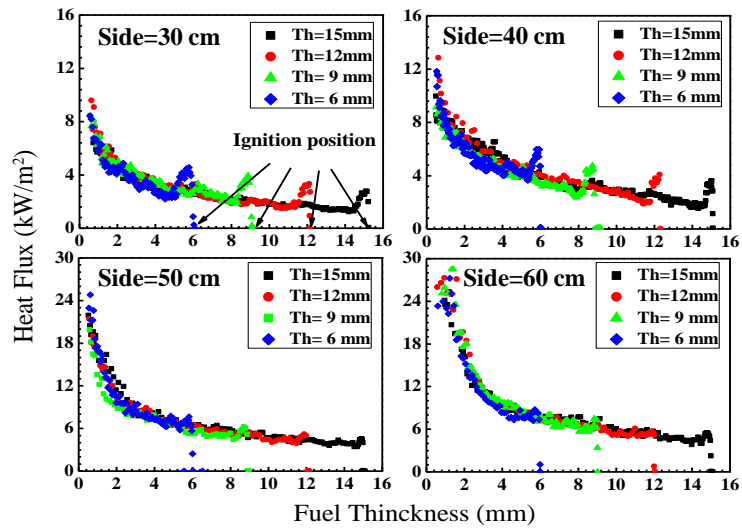
Fig. 8 The PHF variation vs. the fuel thickness at the center position. Th is the initial fuel thickness and Side is the side length of trays.
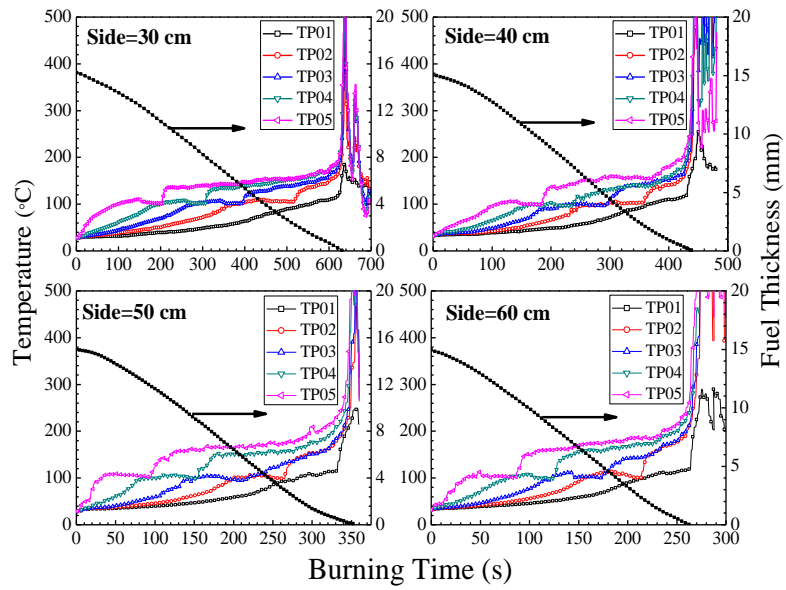
Fig. 9 The fuel and gas temperature and the fuel thickness variation vs. the burning time. Side is the

side length of trays.
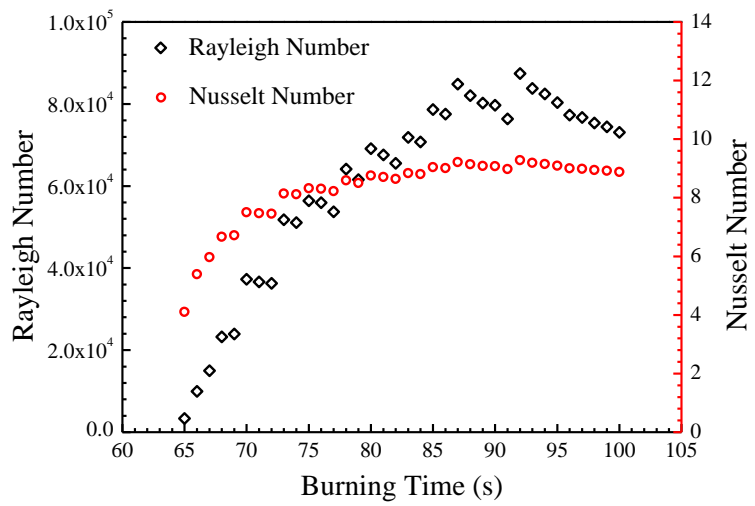
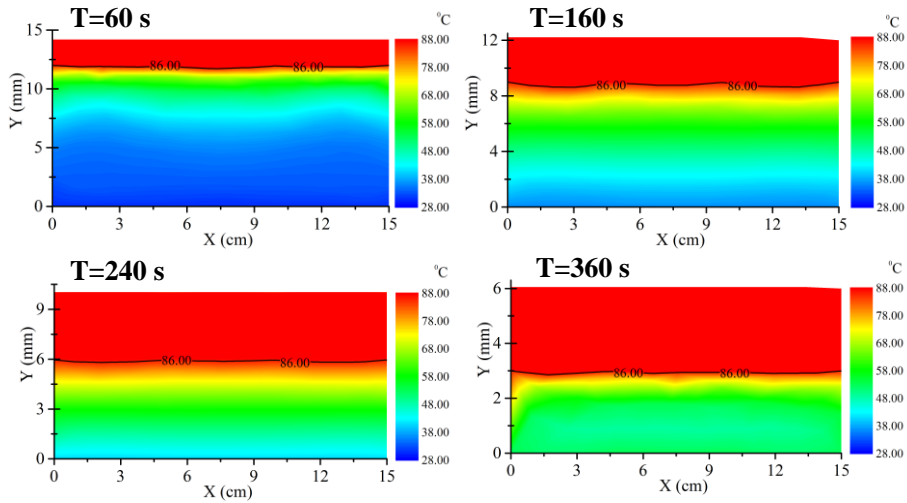Fig. 10 The change in Rayleigh number and Nusselt number over burning time.

Fig. 11 The thickness of the boiling layer in Test 1. The initial fuel thickness is 15 mm and the side length of the tray is 30 cm.
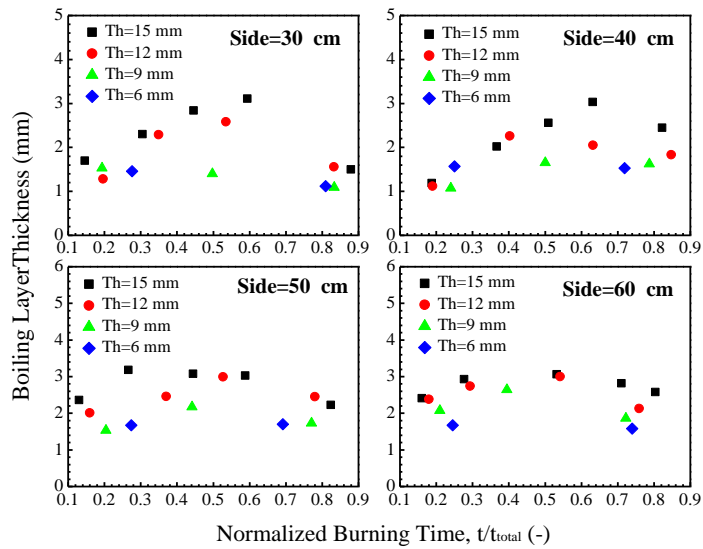

Fig. 12 The thickness variation of the boiling layer over the burning time. Side is the side length of
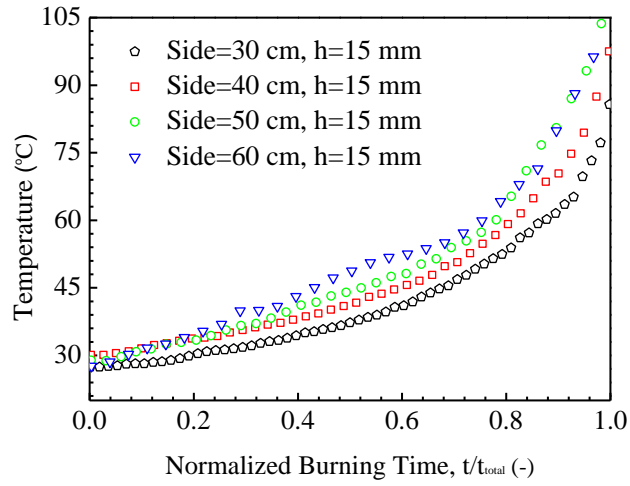
trays.

Fig. 13 The temperature variation of the center bottom glass with the burning time. Side is the side length of trays.
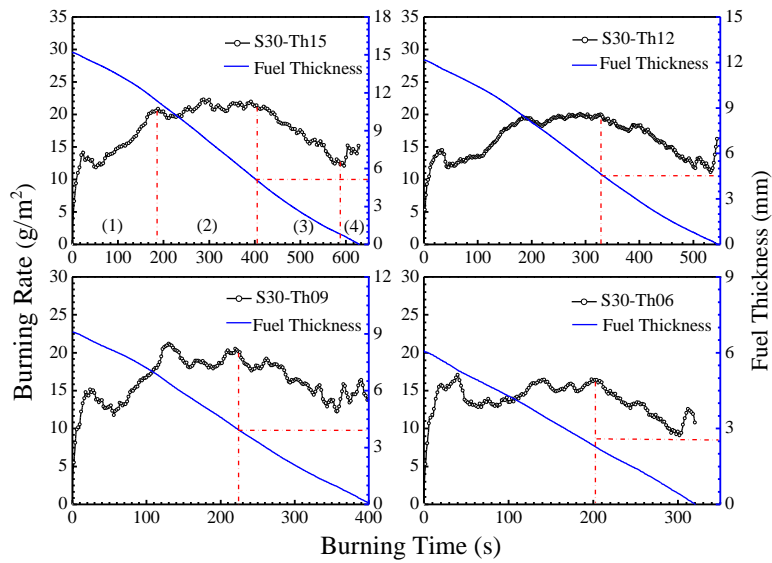

Fig. 14 Burning rate and fuel thickness vs. burning time. The side length of the tray is 30 cm.